King Saud University

Arabian Journal of Chemistry

www.ksu.edu.sa
www.sciencedirect.com

ORIGINAL ARTICLE

A novel radial basis Bayesian regularization deep neural network for the Maxwell nanofluid applied on the Buongiorno model

Zulqurnain Sabir [a], Nevzat Akkurt [b], Salem Ben Said [a,*]

[a] Department of Mathematical Sciences, UAE University, P. O. Box 15551, Al Ain, United Arab Emirates
[b] Munzur University, Rare earth elements Application and Research Center, 62000, Tunceli, Turkey

Abstract The aim of this work is to provide the numerical solutions of the fluid model by using the stochastic computing paradigms. The linear/exponential stretching sheets on magneto-rotating flow based on the Maxwell nanofluid have been provided using the Buongiorno model with the impacts of uneven heat source/sink, varying thermal conductivity and reactive species. The solutions of this transformed ordinary differential exponential stretching sheet model have been presented using a novel 'radial basis' (RB) activation function together with the Bayesian regularization deep neural network (BRDNN), i.e., RB-BRDNN. The deep neural network is presented into two hidden layers, while thirteen and twenty-five numbers of neurons have been used in the first and second layer. A reference dataset is proposed using the Runge-Kutta scheme for the model. The correctness of the stochastic RB-BRDNN procedure is examined through the comparison of proposed and database results, whereas minimal absolute error values provide the accuracy of the scheme. The reliability and competence of the computing RB-BRDNN solver is authenticated using the state transitions, correlation, regression, and error histograms.

1. Introduction

Non-Newtonian fluids (NNFs) have huge importance because of the variety of industrial and engineering applications, some of them are polymer, petroleum, chemical engineering, and food processing industries. These models also arise in the motor oils, biological fluids, complex mixtures, pastes, polymeric liquids, and slurries. Several NNFs represent the nonlinear behavior between strain and stress. The process known as stress relaxation when the shear strains are reduced. Recently, Maxwell fluid (MF) model is known as one of NNFs that has been studied by various scholars. Maxwell (Maxwell, 2003) proposed the elastic and viscous impacts of air based on MF model. An exponentially extending layer was used by Singh et al (Singh and

ELSEVIER | **Production and hosting by Elsevier**

Nomenclature

Ω	Angular velocity	D/Dt	Material derivative
u, v, w	Velocities	ρ	Fluid density
T_w	Convective surface	D_T	Thermophoresis coefficient
T_∞	Ambient fluid temperature	K	Chemical reaction constant
C_w	Sheet surface	τ^*	Particle to fluid capacity
C_∞	Ambient concentration	ρc_p	Heat capacitance
S	Extra stress tensor for MF	T	Temperature
A_1	Rivlin-Ericksen tensor	K	Thermal conductivity
μ	Viscosity	$k(T)$	Variable thermal conductivity
D_1, D_2, E_1, E_2 Constants		k_∞	Ambient thermal conductivity
V_T	Thermophoretic velocity	$v_t\, k_1^*$	Thermophoretic coefficients
T_r	Reference temperature	q'''	Uneven heat sink/source
ε	Thermal conductivity	A^*, B^*	Space and temperature coefficients
q_{rad}	Radiative heat flux	P and Q	Temperature and concentration exponents
$f(\eta),\, g(\eta),\, \theta(\eta),\, \varphi(\eta)$ Dimensionless variables		β	Rotation parameter
λ	Relaxation parameter	R	Radiation parameter
M	Magnetic field parameter	Ec_1, Ec_2	Eckert number in x and y directions
Pr	Prandtl number	S_1 and S_2	Thermal and concentration stratification parameters
Nt and Nb Thermophoresis and Brownian motion parameters			
Sc	Schmidt number	τ	Thermophoretic parameter
α	Stretching ratio parameter	Γ	Concentration difference parameter
λ_1	Relaxation time		

Agarwal, 2014) evaluated the Magnetohydrodynamic (MHD) heat transfer along with MF flow in a porous media under the varying heat capacity. Nadeem et al. (Nadeem et al., 2014) considered the MHD boundary flow based on the MF produced by the stretching a surface based on the nanoparticles. In their discussion of MHD flow, the increasingly stretched sheet behavior is noticed. Farooq et al. (Farooq et al., 2019) employed the Buongiorno system. Ali et al. (Ali et al., 2019) signified the analysis using the heat/mass transport-based MF using an exponentially extending sheet. For the mass/heat transfer based on MF flow at a stagnation point using the slip condition, Khan et al. (Khan et al., 2019) proposed a stretched surface. The bio-convective MF across the exponentially stretched surface was explained by Khan et al (Khan and Nadeem, 2020). Three dimensional bioconvective MF flow past on an exponentially stretching surface with chemical reaction and variable thermal conductivity is presented by Ahmed et al (Ahmad et al., 2022; Khan et al., 2021). Analysis of irreversibility using the Ellis hybrid nanofluid along with the reaction of surface catalyzed and the impacts of multiple slip past on the porous horizontal cylinder is proposed by Khan et al (Khan et al., 2022). Bio-convective natural MF past on a stretching surface along with the convective boundary condition and slip impacts is studied by Wang et al (Wang et al., 2022). Joule heating and compound slips based on MF over a slandering surface is proposed by Ahmed et al (Ahmad et al., 2021). The chemical reactive type of species in MF is presented by Nadeem et al (Nadeem et al., 2017).

The steady/unsteady rotational flow have frequent applications in the chemical/geophysical fluids along with various industries including generation of thermal power, food processing, high-speed aircraft cooling and rotating machinery. Nazar et al. (Nazar et al., 2004) applied a similarity technique to evaluate the unstable boundary layer based on the rotating fluid flow past on a stretching sheet. A mathematical concept of rotating fluid past a stretching sheet was initially addressed by Wang (Wang, 1988). Shafique et al. (Shafique et al., 2016) examined the mass/heat transfer using the rotating MF flow on a stretched sheet with an activation energy. Ibrahim et al. (Ibrahim and Seyoum, 2019) proposed the characteristics of the heat transfer using the Sisko fluid in

the rotational frame. Rashid et al. (Rashid et al., 2020) discussed the boundary layer over a stretching sheet of a spinning Maxwell nanoparticle using the activation energy. By employing the Buongiorno system, Ahmed et al. (Ahmed et al., 2020) examined the mixed convective boundary layer MF flow using a vertical rotational cylinder. Hafeez et al. (Hafeez et al., 2020) investigated the stagnation point with Oldroyd-B flow using the thermal radiation. Ferrofluid uses with electric field insertion inside a porous cavity to assume the forced convection is studied by Shah et al (Shah and Ullah, 2023). Computational investigations and magnetized gold-blood Oldroyd-B characteristics and heat transfer are presented by Tang et al (Tang et al., 2023). Magnetized mixed convection hybrid nanofluid using the heat absorption/-generation effects along with the conditions of velocity slip are presented by Asghar et al (Asghar et al., 2023). Hybridized nanofluid flow along a triangular-molded obstacle within a splitting lid-driven trapezoidal space is presented by Khan et al (Khan et al., 2022; Khan et al., 2022). In another study, Khan et al (Khan et al., 2022) proposed the flow based on the double-diffusion using a porous trapezoidal field with constant heat flux. The natural convection in an angled trapezoidal space with sinusoidal wall temperature is also provided by Khan et al (Khan et al., 2021; Khan et al., 2020).

Stratification is such a phenomenon that is caused by changing the concentration, temperature, or the presence of fluids based varying proportion. Waves evolution inside the air circulation across the mountains and haze in the air are two examples of stratification that affect the environment. The operation of biological systems prohibits the thermal boundary layer thickness from causing the bottom water. Since it is adjusted the temperature/concentration based on the hydrogen/oxygen, which can be hazardous for the evolution of aquatic life. The stratification phenomena arise in the geophysical flows, e.g., reservoirs of ground water, seas, lakes, and rivers. The significance of both nature and industry, stratification has drawn the attention of numerous scientists. The convective heat transfer based on the micropolar fluid was produced by Cheng et al. (Chang and Lee, 2008) along with uniform and steady heat flux throughout a vertical wall. Mukhopadhyay et al. (Mukhopadhyay and Ishak, 2012) calculated the flow of

mixed convection using the thermal stratification based on the stretching cylinder. Ibrahim et al. (Ibrahim and Makinde, 2013) conducted the nanofluid boundary layer flow, which has an influence through the stratification past on a vertical plate. The flow based on the Darcy-Forchheimer using the MF with binary stratification past on the stretching surface is presented by Lakshmi et al. (Lakshmi et al., 2018). Sandeep et al. (Sandeep and Gnaneswara Reddy, 2017) studied the Oldroyd-B fluid using the double stratification passing on a melting surface. Tlili et al. (Tlili et al., 2020) provided the MF flow using the double stratification passing on a stretching surface. The boundary layer flow using the thermal lamination past on a stretching surface is studied by Daniel et al. (Daniel et al., 2018). The estimation of artificial neural network based on the coefficient of skin friction using the cylindrical surface is provided by Rehman et al (Rehman et al., 2023; Rehman et al., 2023). In another study, Rehman et al (Rehman et al., 2023) provided the computational performances using the magnetized/ non-Magnetized boundary layer flow of Casson fluid passing over a cylindrical surface through the artificial neural networks.

The mass/heat transfer presents the natural phenomenon, which has a variety of submissions, e.g., thermal action of pain using the hot bag water, boiling of milk and food cooking using the metal pots. The phenomenon based on the mass transfer arises in various progressions, e.g., mixture thermal insulation concentration, vaporization, food dispensation, absorption, cooling towers and nutrients diffusion in tissues. Hossain et al. (Hossain and Rees, 1999) studied the mass/ heat transfer using the flow of natural convection based on the wavy surface. Khan (Khan et al., 2019) adjusted the transfer of mass/heat examination based on the mixed MHD convection of 2nd grade fluid using the thermophoresis inspiration along with the hall current impacts. In another investigations, Shateyi (Shateyi, 2013) proposed the heat transfer flow based on the MF with chemical reaction and thermophoresis past on a stretching surface. Cu nanoparticles were used to improve the heat transport in a nanofluids based water presented by Saleem et al. (Saleem et al., 2020). Nawaz et al. (Nawaz et al., 2020) examined the characteristics of mass/heat using the boundary layer flow via nonlinear stretching surface with the coefficient of variable diffusion and partial slip. Few more investigations related to this study are presented in these references (Sajid et al., 2020; Ayub et al., 2022; Ayub et al., 2021).

The other paper parts are given as: Section 2 shows the physical problem statement, Section 3 indicates the methodology and validation. Section 4 provides the results and discussions. Conclusions are presented in the last Section.

2. Physical problem statement

The idea of exponential stretchable coaxially rotating sheets in fluid is presented as:

The idea of exponential stretchable coaxially rotating sheets in fluid has significant importance in fluid mechanics, particularly in the study of vortex dynamics and turbulence. Here are some of the reasons why this idea is important:

1. Understanding of vortex dynamics: Coaxial rotation of sheets produces a series of vortices that interact with each other, leading to complex and chaotic flow patterns. The exponential stretching of the sheets leads to a wide range of scales of vortices, which can be studied to gain insights into the complex dynamics of turbulence.
2. Modeling of real-world flows: The behavior of fluids in many real-world situations, such as the flow around aircraft wings or the behavior of fluids in the Earth's atmosphere, is highly turbulent and difficult to model accurately. The study of exponential stretchable coaxially rotating sheets

provides a simplified model for these flows, allowing researchers to gain insights into the underlying physics of turbulence.
3. Potential for technological applications: The insights gained from the study of exponential stretchable coaxially rotating sheets can be applied to the design of a wide range of technological applications, such as the design of more efficient aircraft or the optimization of wind turbines.
4. Development of new mathematical techniques: The study of the complex behavior of fluids in exponential stretchable coaxially rotating sheets requires the development of new mathematical techniques, which can have applications in many other areas of mathematics and physics.

2.1. Physical description

The Buongiorno model MF flow from a linear and exponential stretchable coaxially rotating sheets using the heat source/sink, variable reactive species and variable thermal conductivity is considered. In construction of the mathematical model, the flow is controlled to $z \geqslant 0$ with angular velocity Ω as depicted in the Fig. 1. The fluid stretching velocities are taken as u, v and w in the **x** direction conjecture as $u_w = ax, u_w = a\,e^{x/l}$, in the **y** direction are conjecture as $v_w = by$, $v_w = b\,e^{x/l}$ $(a, b > 0)$ based on the linear/exponential sheets. The convective surface is T_w, while the fluid's ambient temperature of fluid is taken as T_∞. The sheet surface is C_w and the ambient concentration is represented by C_∞, the boundary layer laminar flow contains $z > 0$. The extra stress tensor for MF is **S**, which is defined as (Khan and Nadeem, 2021):

$$\left(1 + \lambda_1 \frac{D}{Dt}\right)\mathbf{S} = \mu\,A_1,\tag{1}$$

In the above equation, Rivlin-Ericksen tensor (A_1), viscosity (μ), relaxation time (λ_1), and material derivative (D/Dt). With the assumptions of equation of continuity, equation of momentum, equation of energy and mass for the three-dimensional Maxwell Buongiorno model boundary layer nanofluid flow are achieved to combine the previous system (Khan and Nadeem, 2021) as follows:

$$u_x + u_y + u_z = 0,\tag{2}$$

$$
\begin{aligned}
&\left(u\,u_x + v\,u_y + w\,u_z - 2\,\Omega\,v\right)\\
&= \frac{\mu}{\rho}u_{zz} - \frac{\lambda_1}{\rho}\left\{\begin{array}{c} 2\,\Omega\left(v\,u_x - v\,v_y\right) - 2\Omega(u\,v_x + u\,u_y) + \\ 2\left(u\,v\,u_{xy} + u\,w\,u_{xz} + v\,w\,u_{yz}\right) + u^2\,u_{xx} + \\ v^2\,u_{yy} + w^2\,u_{zz} - 2\,\Omega\,w\,v_z \end{array}\right\}\\
&\quad - \frac{\sigma\,B_0^2}{\rho}u - \frac{\sigma\,B_0^2}{\rho}\,\lambda_1\,w\,u_z,
\end{aligned}
\tag{3}
$$

$$
\begin{aligned}
&\left(u\,v_x + v\,v_y + w\,v_z - 2\,\Omega\,u\right)\\
&= \frac{\mu}{\rho}v_{zz} - \frac{\lambda_1}{\rho}\left\{\begin{array}{c} u^2\,v_{xx} + 2\,\Omega\left(v\,u_y + u\,u_x\right) + v^2\,v_{yy} + \\ 2\,u\,v\,v_{xy} + 2\,w\left(u\,v_{xz} + v\,v_{yz}\right) + 2\,\Omega\,w\,u_z + \\ 2\,\Omega\left(v\,v_x - u\,v_y\right) + w^2\,v_{zz} \end{array}\right\}\\
&\quad - \frac{\sigma\,B_0^2}{\rho}v - \frac{\sigma\,B_0^2}{\rho}\,\lambda_1\,w\,v_z,
\end{aligned}
\tag{4}
$$
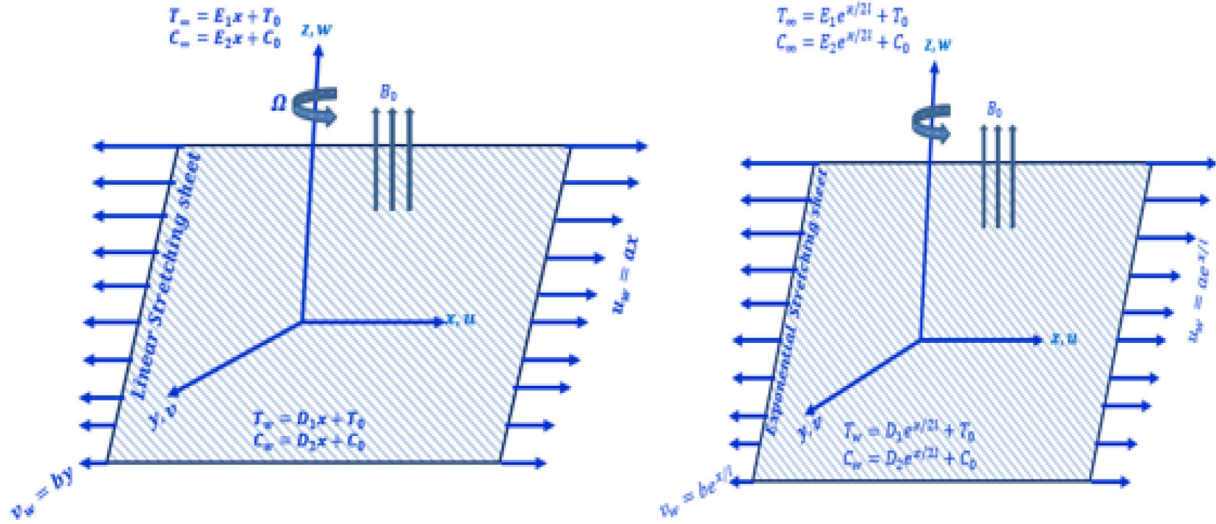
Fig. 1 Physical model for linear and exponential stretching sheet.

$$(u\,T_x + v\,T_y + w\,T_z) = \frac{1}{\rho c_p}(k(T)\,T_z)_z$$
$$+ \frac{q'''}{\rho c_p} - \frac{(q_{rad})_z}{\rho c_p} + \mu(\rho c_p)^{-1}\{(v_z)^2 + (u_z)^2\}$$
$$+ \frac{\tau^*}{\rho c_p}\left\{\frac{D_T}{T_\infty}(T_z)^2 + D_B\,T_z\,C_z\right\}, \tag{5}$$

$$u\,C_x + v\,C_y + w\,C_z + (V_T C)_z$$
$$= D_B\,C_{zz} + \frac{D_T}{T_\infty}\,T_{zz} - K(C - C_\infty)^n. \tag{6}$$

The boundary conditions (BCs) on linear sheet are given as:

$$\left.\begin{array}{c}
\text{at } z \to 0; \quad v = v_w(x),\ u = u_w(x),\ w = 0, \\
T_w = T = T_0 + D_1\,x,\ C_w = C = C_0 + D_2\,x \\
\text{at } z \to \infty; \quad v \to 0,\ u \to 0, \\
T \to T_\infty = T_0 + E_1\,x, \qquad C \to C_\infty = C_0 + E_2\,x
\end{array}\right\} \tag{7}$$

The BCs on exponential sheet are:

$$\left.\begin{array}{c}
\text{at } z \to 0;\ v = v_w(x),\ u = u_w(x),\ w = 0, \\
T_w = T = T_0 + D_1\,e^{x/2l},\ C_w = C = D_2\,e^{x/2l} + C_0 \\
\text{at } z \to \infty;\quad u \to 0,\ v \to 0, \\
T \to T_\infty = T_0 + E_1\,e^{x/2l},\ C \to C_\infty = C_0 + E_2\,e^{x/2l}
\end{array}\right\} \tag{8}$$

where μ denotes the viscosity, ρ represents fluid density, D_T denotes the thermophoresis coefficient, K denotes chemical reaction constant, τ^* denotes ratio of particle to fluid capacity, ρc_p denotes the heat capacitance, T denotes the temperature, k denotes the thermal conductivity. Further, D_1, D_2, E_1 and E_2 denote the positive constants. The variable thermal conductivity $k(T)$ and the thermophoretic velocity V_T are modelled with the following equations (Khan et al., 2017):

$$\begin{cases} k(T) = k_\infty\left\{1 + \varepsilon\left(\frac{T - T_\infty}{T_w - T_0}\right)\right\}, \\ V_T = -\frac{v_t\,k_1^*}{T_r}(T_z). \end{cases} \tag{9}$$

Where k_∞ denotes the ambient thermal conductivity, T_r is the reference temperature, $v_t\,k_1^*$ shows the thermophoretic coefficient, and ε presentes the thermal conductivity. q''' is uneven heat sink/source and q_{rad} shows the net radiative flux of heat using as (Sulochana et al., 2017):

$$q''' = \frac{k\,u_w}{x\,v}(T_w - T_0)\{A^*f' + B^*(\frac{T-T_\infty}{T_w-T_0})\},$$
$$(q_{rad})_z = -\frac{16\,\sigma^*}{3k^*}(T^4)_{zz} = --\frac{16\,\sigma^*\,T_\infty^3}{3k^*}(T)_{zz}. \tag{10}$$

A^* and B^* are the coefficients of space and temperature dependent based on the heat or sink source. σ^* and k^* indicate the Stefan-Boltzmann radiation constant and mean absorption coefficient. The applicable similarity form is provided as (Khan and Nadeem, 2021):

For linear sheet

$$v = a\,x\,g(\eta),\ u = a\,x\,f'(\eta),\ \eta = \sqrt{\frac{a}{v}}z,\ w = -\sqrt{a\,v}f(\eta),$$
$$T = T_\infty + T_w\,\theta(\eta) - T_0\,\theta(\eta),\ C = C_\infty + C_w\,\varphi(\eta) - C_0\,\varphi(\eta). \tag{11}$$

For exponential Sheet

$$u = a\,e^{x/l}f'(\eta),\quad v = a\,e^{x/l}g(\eta),\quad w = -\sqrt{\frac{a\,v}{2l}}e^{x/2l}\{f(\eta) + \eta\,f'(\eta)\},$$
$$T = T_\infty + A_0\,e^{Px/2l}\,\theta(\eta),\quad C = C_\infty + B_0\,e^{Qx/2l}\,\varphi(\eta),\quad \eta = \sqrt{\frac{a}{2\,l\,v}}z. \tag{12}$$

Where $f(\eta)$, $g(\eta)$, $\theta(\eta)$ and $\varphi(\eta)$ are dimensionless variables with similarity variable η, further, P and Q are the exponents of temperature and concentration, while A_0 and B_0 are the positive constants. Using the Eqs. (9 to 12) in Eqs. (2 to 8), the transformed momentum, energy, and mass equations at linear and exponential sheet with corresponding BCs are as follows:

For linear sheet

$$f''' - 2\lambda\beta fg' + ff'' - \lambda(f^2f''' - 2f''ff') + 2\beta g - (f')^2$$
$$- M\alpha f''f' - Mf' = 0, \tag{13}$$

$$(1 - \lambda f^2)g'' - 2\beta f' + 2\lambda g'ff' - 2\beta(\lambda g^2 + \lambda f'^2 - \lambda f''f + f') - gf'$$
$$+ (1 - M\lambda)fg' - Mg = 0, \tag{14}$$

$$(1 + \varepsilon\theta + R)\theta'' + Pr\{f\theta' - f'\theta + Ec_1f''^2 + Ec_2g'^2 + Nt\theta'^2 + Nb\theta'\varphi' - S_1f'\}$$
$$+ (1 + \varepsilon\theta)(A^*f' + B^*\theta - A^*S_1f') + \varepsilon\theta'^2 = 0, \tag{15}$$

$$\varphi'' + Sc\{f\varphi' - f'\varphi\} - Sc\,\tau(\theta'\varphi' - \Gamma\theta'' - \varphi\theta'') + \frac{Nt}{Nb}\theta''$$
$$- Sc\,S_2 f' - Sc\,K_c\varphi^n = 0 \tag{16}$$

For exponential sheet

$$f''' + (1 + 3\lambda f')ff'' - (4\lambda f' + 2)f'^2 - Mf' - 2\lambda(fg' + \eta f''g) + 4\beta g$$
$$-0.5\lambda(f^2 f''' - \eta f'' f'^2) - M\lambda ff'' = 0, \tag{17}$$

$$g'' + 3\lambda ff'g' - 2gf' - 2\lambda f'^2 g - 0.5\lambda(f^2 g'' - \eta f'^2 g') + fg'$$
$$-4\beta(f' - (\frac{\eta f'}{2} - f'^2 - \frac{\eta}{2}gg' - g^2)\lambda) - Mg - M\lambda fg' = 0, \tag{18}$$

$$(1 + \varepsilon\theta + R)\theta'' + Pr\{f\theta' - Pf'\theta + Ec_1 f''^2$$
$$+Ec_2 g'^2 + Nt\theta'^2 + Nb\theta'\varphi' - S_1 f'\}$$
$$+(1 + \varepsilon\theta)(A^* f' + B^*\theta - A^* S_1 f') + \varepsilon\theta'^2 = 0, \tag{19}$$

$$\varphi'' + Sc\{f\varphi' - Q\,f'\varphi\} - Sc\,\tau(\theta'\varphi' - \Gamma\theta'' - \varphi\theta'') + \frac{Nt}{Nb}\theta''$$
$$- Sc\,S_2 f' - Sc\,K_c\varphi^n = 0. \tag{20}$$

The final BCs in dimensionless form are

$$f(0) = 0, \quad f'(0) = 1, \quad g(0) = \alpha, \quad \theta(0) = 1 - S_1, \quad \varphi(0) = 1 - S_2,$$
$$f'(\eta) = 0, \qquad g(\eta) = 0, \qquad \theta(\eta) = 0, \qquad \varphi(\eta) = 0. \tag{21}$$

The non-dimensional quantities arising in Eqs (13) - (21) are given as:

$$\lambda = a\lambda_1, \quad \beta = \frac{\Omega}{a}, M = \frac{\sigma B_0^2}{a\rho}, \quad R = \frac{16\sigma^* T_\infty^3}{3k_\infty k^*}, Pr = \frac{v}{\alpha_f}, Ec_1 = \frac{u_w^2}{c_p(T_w - T_\infty)},$$
$$Ec_2 = \frac{v_w^2}{c_p(T_w - T_\infty)}, Nt = \frac{\tau^* D_T(T_w - T_\infty)}{vT_\infty}, Nb = \frac{\tau^* D_B(C_w - C_\infty)}{v}, S_1 = \frac{E_1}{D_1},$$
$$Sc = \frac{v}{D_B}, \tau = \frac{-k^*(T_w - T_\infty)}{T_\infty}, \Gamma = \frac{(C_w - C_\infty)}{C_\infty}, S_2 = \frac{E_2}{D_2}, K_c = \frac{K}{a}. \tag{22}$$

The parameters, which are changed in the exponential sheet are:

$$\lambda = \frac{a\,\lambda_1}{l}e^{x/l}, \quad \beta = \frac{\Omega l}{a}e^{x/l}, K_c = \frac{Kl}{a}e^{x/l}, \quad M = \frac{\sigma B_0^2\,l}{a\,\rho}e^{x/l}. \tag{23}$$

Where (λ, β) stands for relaxation and rotation parameters, M is the magnetic field parameter, R denotes the radiation parameter, Pr shows the Prandtl number, Ec_1, Ec_2 are the Eckert number in $\times$ and y directions, Nt and Nb are the thermophoresis and Brownian motion parameters, S_1 and S_2 are the parameters of thermal and concentration stratification, Sc is the Schmidt number, τ shows the thermophoretic parameter, α denotes the Stretching ratio parameter, Γ signifies the concentration difference parameter, K_c and ε are called the chemical reaction and thermal conductivity parameters.

This numerical study provides the solutions of the exponential stretching sheet on magneto-rotating flow of Maxwell nanofluid employed with the Buongiorno model using the impacts of uneven heat source/sink, varying thermal conductivity and reactive species. The ordinary differential exponential stretching sheet model has been solved numerically using a novel radial basis (RB) activation function together with the Bayesian regularization deep neural network (BRDNN), i.e., RB-BRDNN. Recently, there are various differential models that been used to solve by the stochastic computing

schemes, however the exponential stretching sheet model has never been solved through the process of deep neural networks (Sabir, 2022; Umar et al., 2020; Sabir, 2022; Sabir et al., 2021; Sabir et al., 2021; Shah et al., 2023). Few novel features of this work are reported as:

• The linear and exponential stretching sheets on magneto-rotating flow of Maxwell nanofluid employed with the Buongiorno model using the impacts of uneven heat source/sink, varying thermal conductivity and reactive species have been presented.
• The rendered highly nonlinear coupled ordinary differential equations of momentum, energy and mass equations from a Navier-Stokes based partial differential equations have been obtained using the influential similarity transformations.
• The numerical performances of the exponential stretching sheet on magneto-rotating flow of Maxwell nanofluid employed with the Buongiorno model have been presented.
• A novel stochastic computing RB-BRDNN scheme is presented successfully to solve the exponential stretching sheet model.
• The process of RB-BRDNN is provided by using thirteen and twenty-five neurons in hidden layers 1 and 2.
• The procedure's precision is authenticated through the comparison of reference and proposed solutions, while the reduceable absolute error (AE) performances authenticate the exactness of the stochastic procedure.

3. Methodology and validation

The current section presents the process of DNN through the radial basis activation function along with the optimization of Bayesian regularization for the numerical results of fluid dynamics model using the exponential sheet. The process of DNN based on the radial basis activation function is provided mathematically and graphically through the layer construction.

3.1. Radial basis deep learning process

This current section presents the DNN process through the radial basis activation function along with the optimization of Bayesian regularization for the numerical results of fluid dynamics model using the exponential sheet by taking thirteen and twenty-five numbers of neurons in the hidden layer 1 and 2. The feed-forward using the neural network process is presented in three-layer as:

$$\begin{bmatrix} u_1 \\ u_2 \\ u_3 \\ . \\ . \\ . \\ u_{13} \end{bmatrix} = \delta\left(\begin{bmatrix} w_{1,1} \\ w_{1,2} \\ w_{1,3} \\ . \\ . \\ . \\ w_{1,13} \end{bmatrix}[\eta] + \begin{bmatrix} b_{1,1} \\ b_{1,2} \\ b_{1,3} \\ . \\ . \\ . \\ b_{1,13} \end{bmatrix}\right) \tag{24}$$
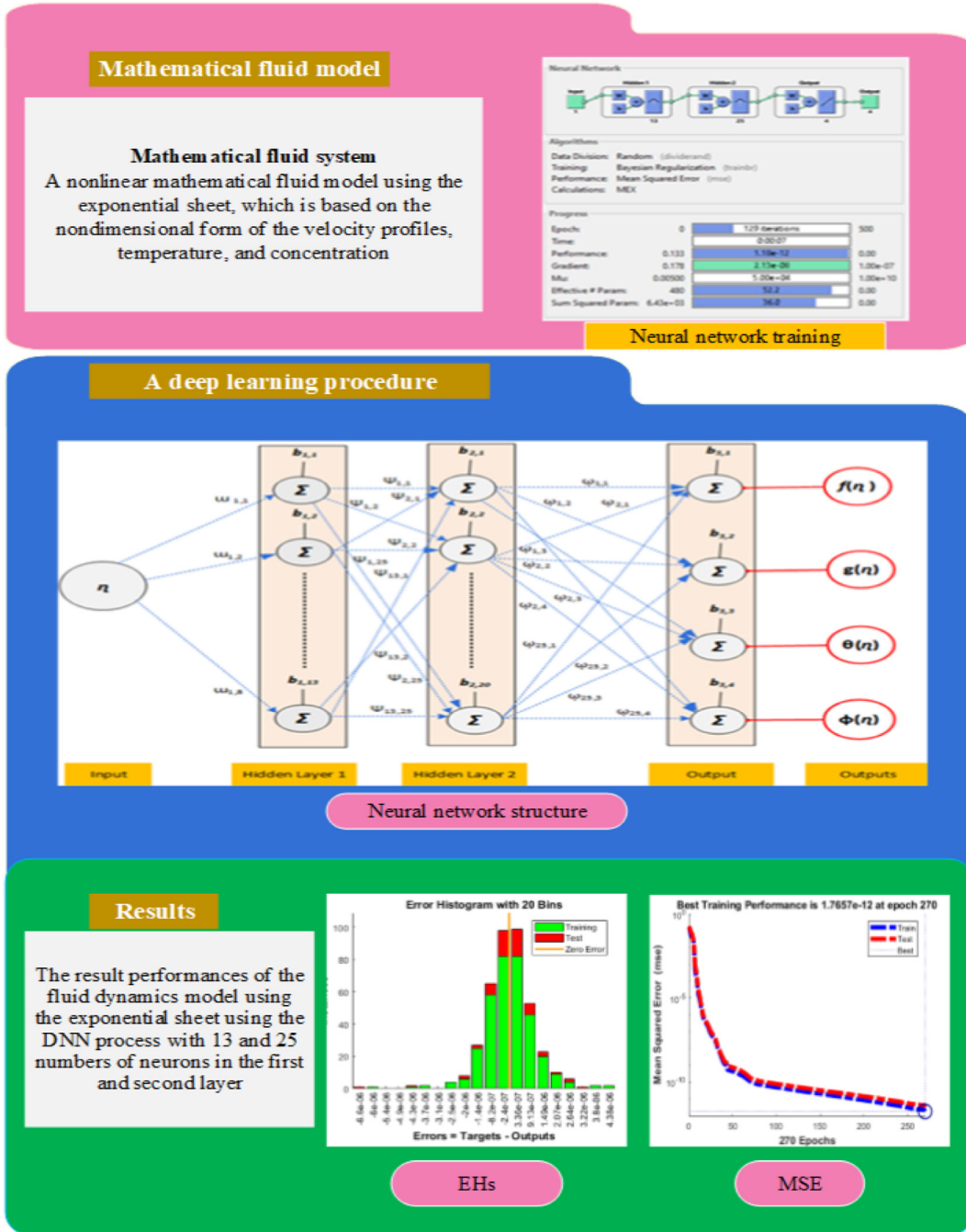
Fig. 2 A layer construction and results routines based on the stochastic scheme.

$$
\begin{bmatrix} v_1 \\ v_2 \\ v_3 \\ . \\ . \\ . \\ v_{25} \end{bmatrix} = \delta \left(\begin{bmatrix} \psi_{1,1} & \psi_{2,1} & \psi_{3,1} & \psi_{4,1} & . & . & w_{13,1} \\ \psi_{1,2} & \psi_{2,2} & \psi_{3,2} & \psi_{4,1} & . & . & w_{13,2} \\ \psi_{1,3} & \psi_{2,3} & \psi_{3,3} & \psi_{4,1} & . & . & w_{13,3} \\ . & . & . & . & . & . & . \\ . & . & . & . & . & . & . \\ . & . & . & . & . & . & . \\ \psi_{1,25} & \psi_{2,25} & \psi_{3,25} & \psi_{4,25} & . & . & w_{13,25} \end{bmatrix} \begin{bmatrix} u_1 \\ u_2 \\ u_3 \\ . \\ . \\ . \\ u_{13} \end{bmatrix} + \begin{bmatrix} b_{2,1} \\ b_{2,2} \\ b_{2,3} \\ . \\ . \\ . \\ b_{2,25} \end{bmatrix} \right)
$$

$$
(25)
$$

$$
\begin{bmatrix} f(\eta) \\ g(\eta) \\ \theta(\eta) \\ \phi(\eta) \end{bmatrix} = \delta \left(\begin{bmatrix} \omega_{1,1} & \omega_{2,1} & \omega_{3,1} & . & . & . & \omega_{25,1} \\ \omega_{1,2} & \omega_{2,2} & \omega_{3,2} & . & . & . & \omega_{25,2} \\ \omega_{1,3} & \omega_{2,3} & \omega_{3,3} & . & . & . & \omega_{25,3} \\ \omega_{1,4} & \omega_{1,4} & \omega_{1,4} & . & . & . & \omega_{25,4} \end{bmatrix} \begin{bmatrix} v_1 \\ v_2 \\ v_3 \\ . \\ . \\ . \\ v_{25} \end{bmatrix} + \begin{bmatrix} b_{3,1} \\ b_{3,2} \\ b_{3,3} \\ b_{3,4} \end{bmatrix} \right),
$$

$$
(26)
$$
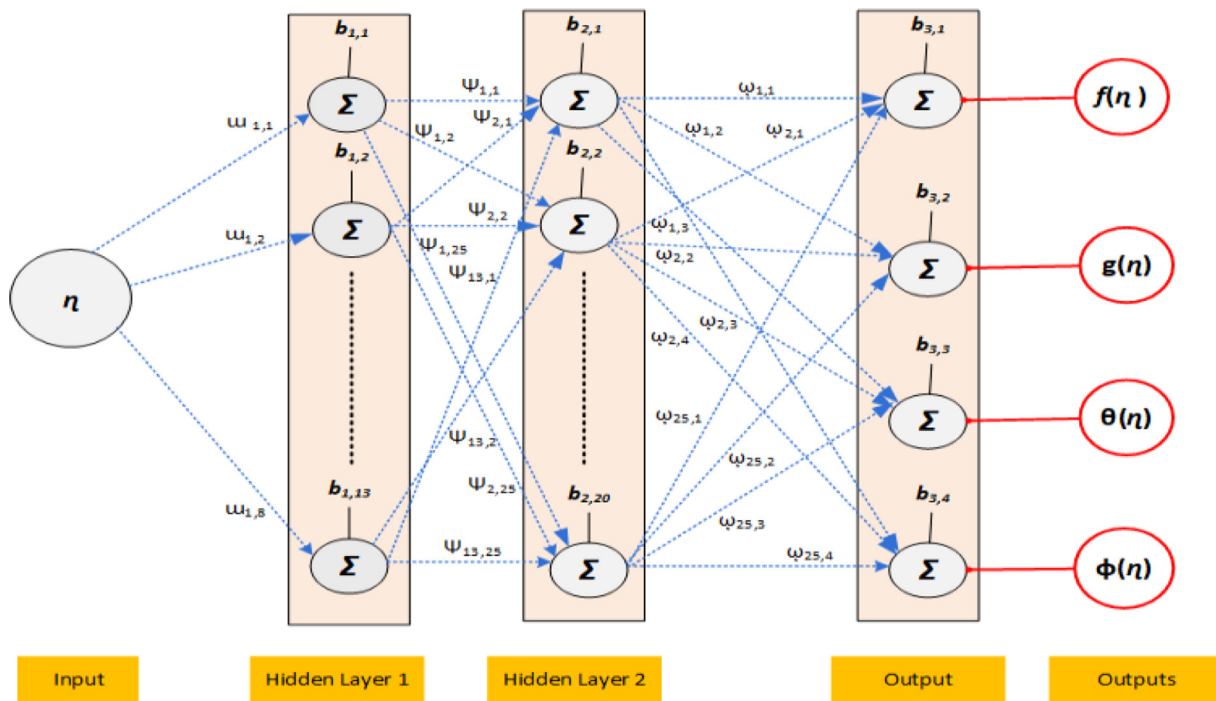
Fig. 3 Multilayer layers procedure for the fluid dynamics model using the exponential sheet.
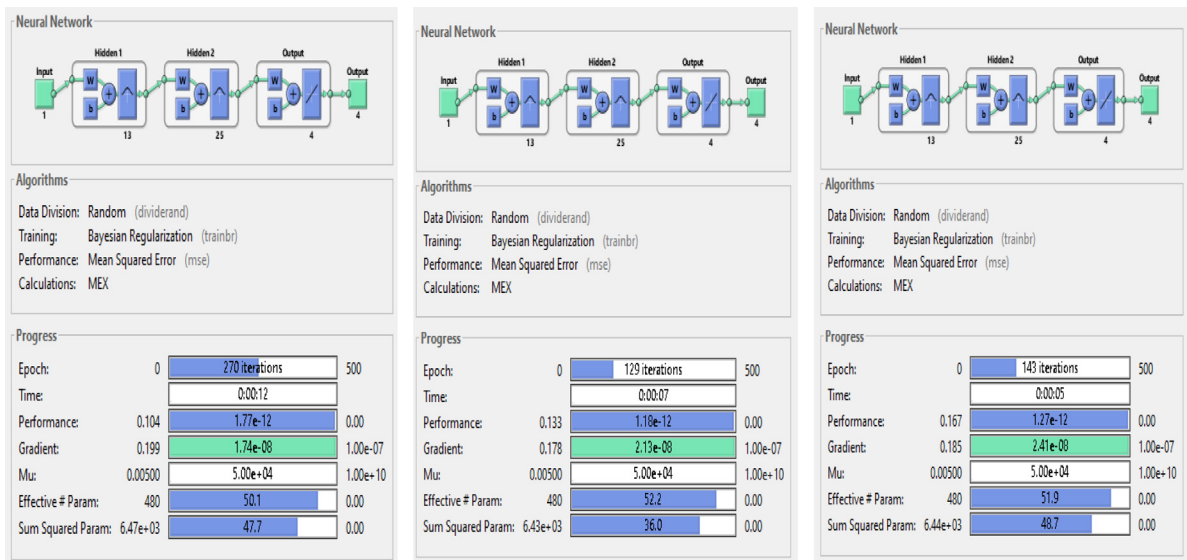
Neural network training for case 1   Neural network training for case 2   Neural network training for case 3

(a) Training of the neural network for each case of the model
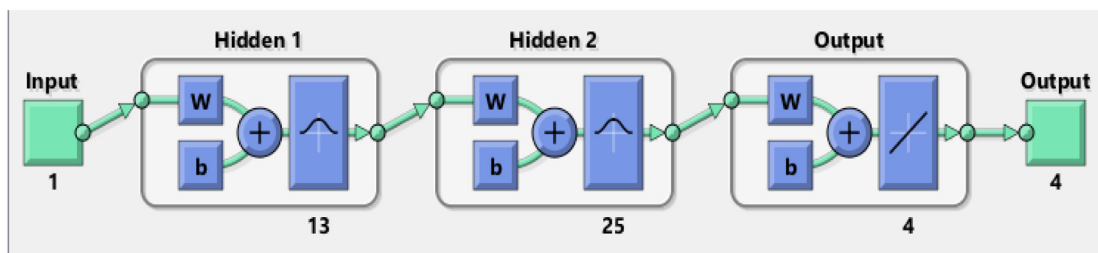
(b) Input, hidden 1-2 and output layers for the model

Fig. 4 Training of the neural network using the DNN for the fluid dynamics model using the exponential sheet.

(a) MSE 1   (b) MSE 2   (c) MSE 3

(d) STs. 1   (e) STs. 2   (f) STs. 3
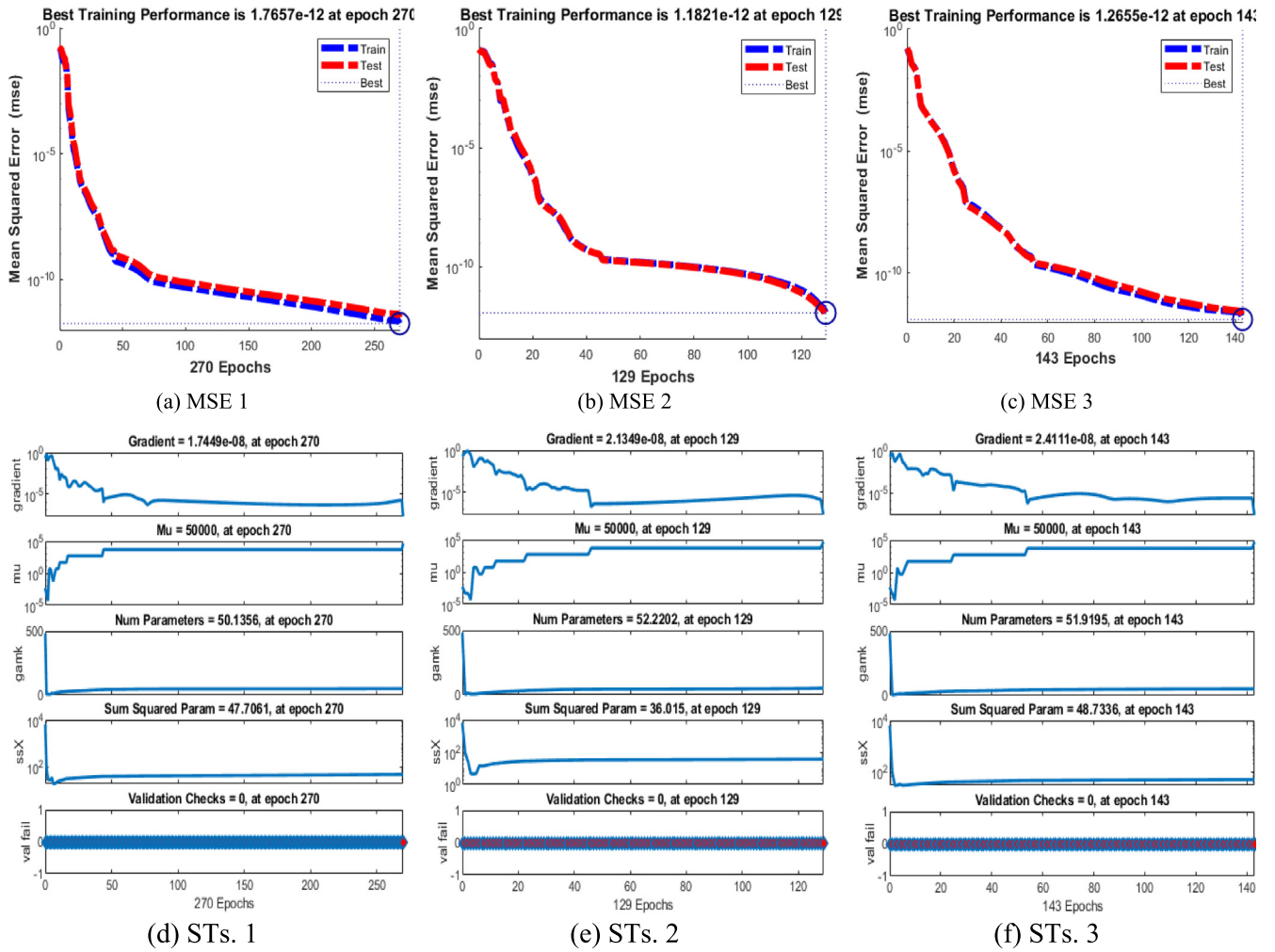
Fig. 5   Graphs through the MSE and STs performances for the fluid dynamics model of exponential sheet.
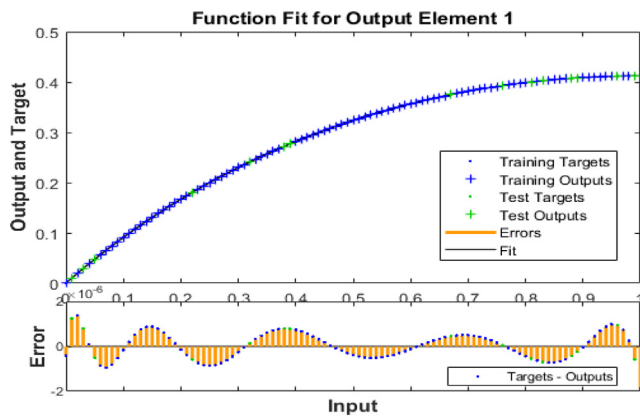
Fig. 6   Fitness for the fluid dynamics model (1) based exponential sheet.
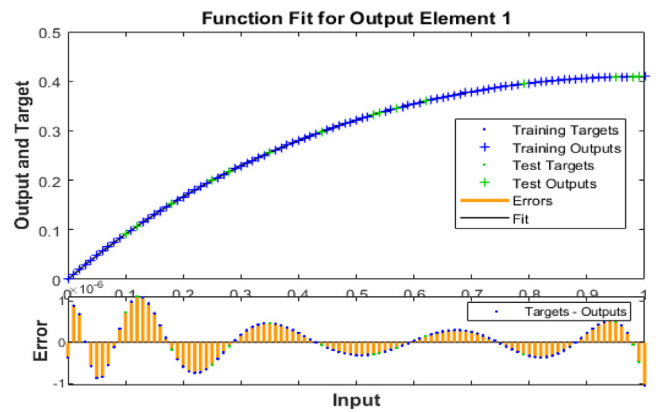
Fig. 7   Fitness for the fluid dynamics model (2) based exponential sheet.
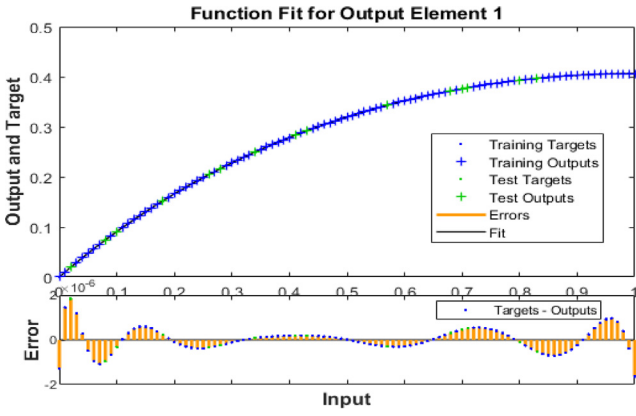
Fig. 8 Fitness for the fluid dynamics model (3) based exponential sheet.

where the weights are represented as w, ψ and ω in the first, second, and output layers. u and v indicate the first and second layers together with output layers $f(\eta)$, $g(\eta)$, $\theta(\eta)$ and $\phi(\eta)$. b indicates the bias and δ is the radial basis activation function, written as:

$$\delta = \exp(-u^2)u = \sum_{i=1}^{n} (w_i\eta_i) + b \qquad (27)$$

where n signifies the number of neurons. Fig. 2 shows the mathematical model, process of neural network, the multi-layer construction along with the obtained performances of the results. A targeted dataset is proposed using the Adam scheme, which is approved further with the training and testing process. Fig. 3 shows the multi-layers procedure based on the single input, two hidden layers with 13 and 25 neurons along with output layers.

Fig. 4 (a) presents the neural network process, the algorithm used for the solution, the Bayesian regularization optimization along with MSE performances. The progress of Epochs that have been selected as 500, time executed, performances, gradient and Mu is also presented for each case of the fluid dynamics model using the exponential sheet. Fig. 4

(b) indicates the DNN performances with 13 and 25 numbers of neurons in the hidden layers.

3.2. Bayesian regularization

The process of Bayesian regularization is applied together with the neural network, which presents the quality of the results in an efficient way despite of other conventional solvers. The Bayesian regularization approach is applied to reduce the lengthy requirement of the cross-validation. This method is documented as a mathematical approach, which alters the performances of the nonlinear regression into the special statistical system through the ridge regression. Recently, Bayesian regularization is implemented in the variety of applications, e.g., measurable susceptibility map rebuilding through MR phase data (De Rochefort et al., 2010), improve the performances in pulse radar detection (Kumar et al., 2004), a comparative empirical study on social data (Kayri, 2016), prediction of austenite formation temperatures (Rakhshkhorshid and Teimouri Sendesi, 2014), and deconvolution for space signal response assessment (Lin and Lee, 2006).

4. Discussion of results

This section presents the numerical performances of the fluid dynamics model by taking three different values of the magnetic parameter $M = 0.1, M = 0.5$ and $M = 0.7$, while the other parameter values have been fixed in the system (17) to (21) as $\lambda = 0.5$, $\beta = 0.3$, $\eta = 0.1$, $\varepsilon = 0.1$, $R = 0.2$, $Pr = 3.5$, $P = 0.3$, $Ec_1 = 0.1$, $Ec_2 = 0.2$, $Nt = 0.1$, $Nb = 0.2$, $S_1 = 0.1$, $A^* = B^* = 0.3$, $Sc = 2.5$, $Q = 2$, $Kc = \alpha = 0.1$ and $\Gamma = 0.2$.

The process of deep neural network (DNN) is presented through the radial basis activation function along with the optimization of Bayesian regularization for the numerical results of fluid dynamics model using the exponential sheet. The input is selected as 0 and 1 with the step size of 0.01. The activation radial basis function is implemented in both form of the hidden layers with thirteen and twenty-five neurons for the numerical performances of fluid dynamics system using the exponential sheet. Fig. 5 shows the mean square

| (a) EHs. 1 | (b) EHs. 2 | (c) EHs. 3 |
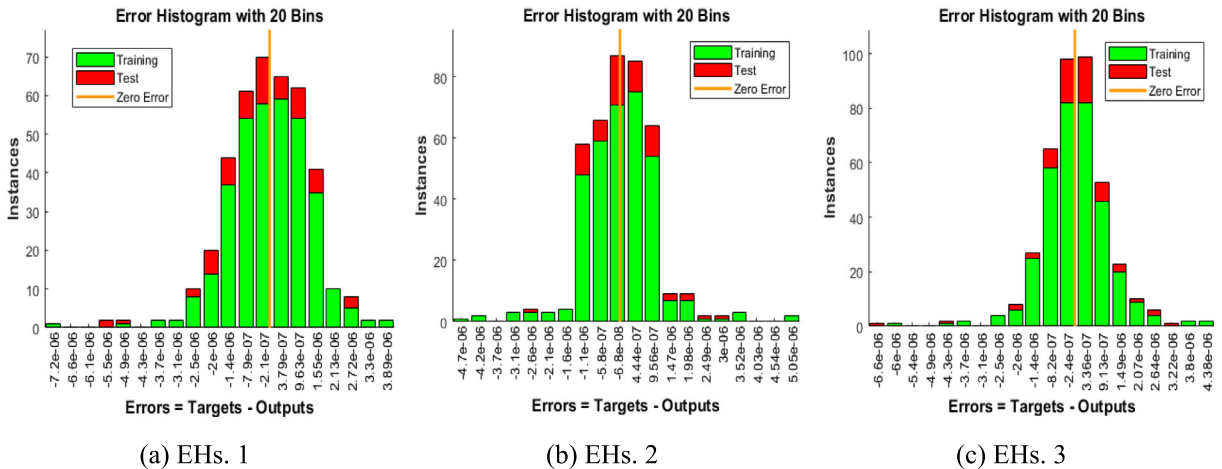
Fig. 9 EHs for the fluid dynamics model based exponential sheet for cases 1 to 3.
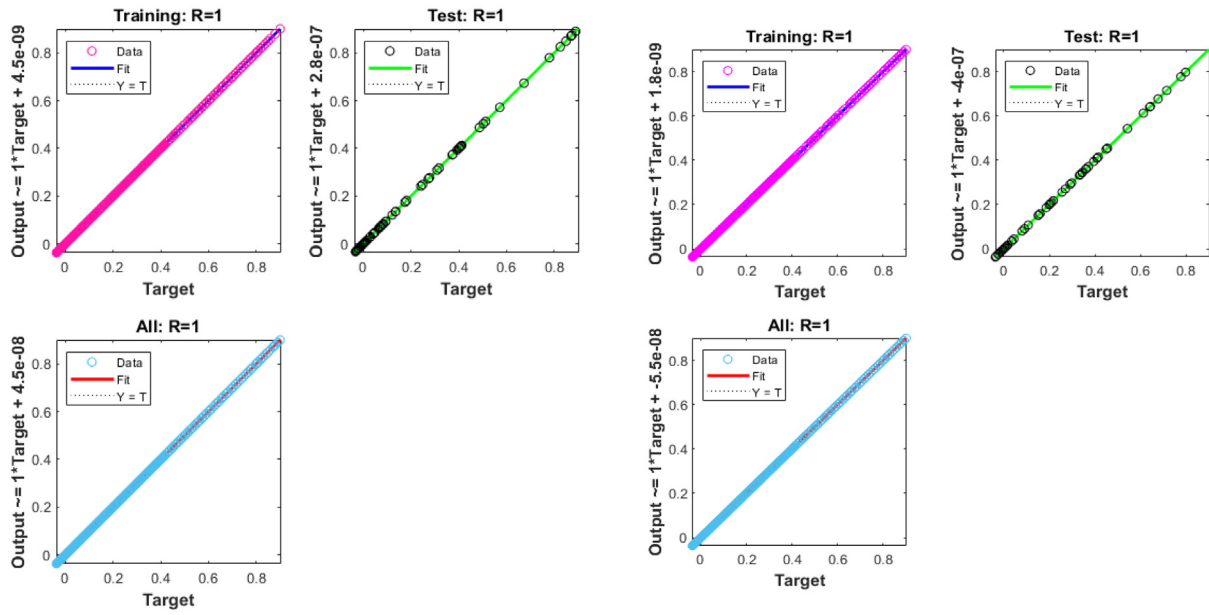
(a) Regression. 1   (b) Regression. 2
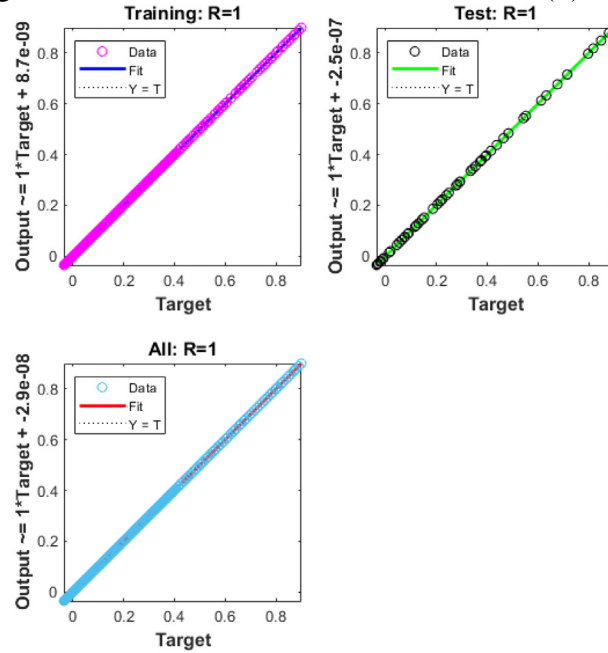
(c) Regression. 3

Fig. 10   Regression for the fluid dynamics model based exponential sheet for cases 1 to 3.

Table 1   DNN process for the fluid dynamics model using the exponential sheet.

Case	MSE		Performance	Gradient	Epoch	Time
	Train	Test				
1	1.7657×10^{-12}	3.0779×10^{-12}	1.77×10^{-12}	1.74×10^{-08}	270	12 Sec
2	1.1821×10^{-12}	9.4363×10^{-13}	1.18×10^{-12}	2.13×10^{-08}	129	07 Sec
3	1.2655×10^{-12}	2.0271×10^{-12}	1.27×10^{-12}	2.41×10^{-08}	143	05 Sec

(a) Comparison. Case 1   (b) Comparison. Case 2   (c) Comparison. Case 3
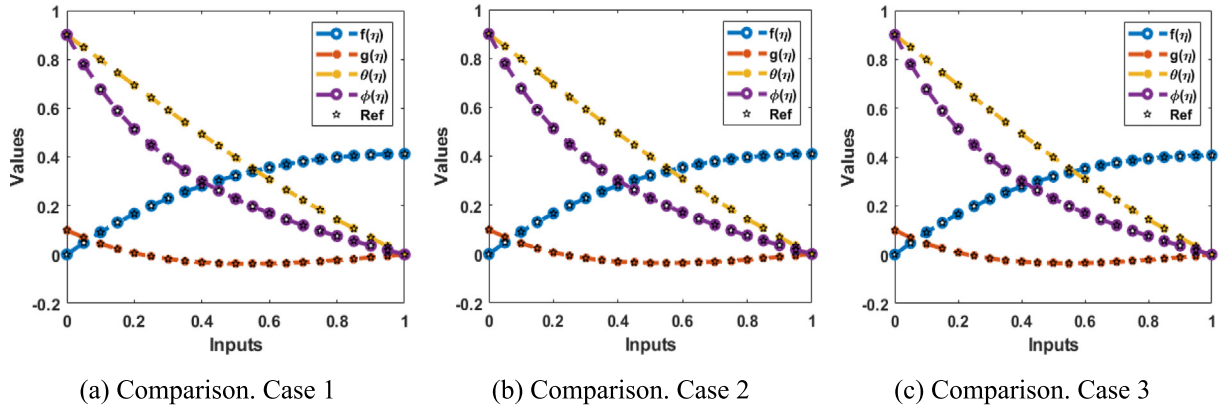
Fig. 11 Comparison performances for the fluid dynamics model based exponential sheet.

error (MSE) and state transitions (STs) values for solving the fluid dynamics system using the exponential sheet. This figure depicts the convergence through MSE based on the dataset of validation, testing, training. It is examined that by increasing the Epochs, the curves based on the validation, training, and testing scheme to steady state point up to 10^{-12}. The selection of epochs has been taken 500 for each case of the model. MSE performances are provided in Fig. 5 that are performed as 1.7657×10^{-12}, 1.1821×10^{-12} and 1.2655×10^{-12} at epochs 270, 129 and 143. Fig. 5 authenticates the num parameters, gradient, sum squared, Mu, and authentication checks. The gradient values are indicated in Fig. 5, which are found as 1.7449×10^{-08}, 2.1349×10^{-08} and 2.4111×10^{-08}. An error form of the gradient shows the magnitude and direction. It is calculated through the designed neural network training, which is applied to enhance the weights of the network in the right amount and direction. In the neural network fitting, backpropagation calculates the loss function gradient relating to network weights based on the example of single input/output effectively, disparate a simple direct calculation of the gradient relating to each weight. Mu shows the obtained training, which stands for momentum parameter or constant including the updated weights to prevent the local minimum problem. Occasionally network can stop to the local minimum and does not converge. It estimates the Hessian matrix inverse that is considered a complex function. Mu represents the control algorithm parameter that is used in the training of neural network. Figs. 6-8 are the function fitness using the DNN through the radial basis activation function along with the optimization of Bayesian regularization for the numerical results of fluid dynamics model for the exponential sheet. Fig. 9 indicates the performances of error histograms (EHs) values by applying DNN through the radial basis activation function along with the optimization of Bayesian regularization for the numerical results of fluid dynamics model using the exponential sheet. The values of the EHs are performed as 3.79×10^{-07}, -6.80×10^{-08} and 3.36×10^{-07}. EHs is created to verify the errors between predicted and targeted performances after training the proposed neural network. These errors represent how projected performances differ through the targeted measures. Fig. 10 represents the regression measures for 1st to 3rd case of the fluid dynamics model using the exponential sheet. R presents the correlation coefficient, which is applied together with MSE based on the performance indexes of neural networks. The values of R vary between -1 and $+1$, while, if R performs close to $+1$, high network performance and a positive linear relationship can be achieved. These values are performed as 1 that indicates the perfect modelling. The train/test data based MSE are tabulated in Table 1 for the fluid dynamics model using the exponential sheet.

Fig. 11 provides the comparison of the outcomes for f, g, θ and ϕ classes of the fluid dynamics model based exponential sheet. The correctness of the scheme is observed through the matching of these solutions for solving the fluid dynamics

Table 2 AE for the classes f, g, θ and ϕ of the fluid dynamics model.

| | AE | | | | | | | | | | |
	0	0.1	0.2	0.3	0.4	0.5	0.6	0.7	0.8	0.9	1
f	4×10^{-7}	2×10^{-7}	1×10^{-7}	3×10^{-7}	7×10^{-7}	4×10^{-7}	1×10^{-7}	5×10^{-7}	4×10^{-7}	3×10^{-8}	2×10^{-6}
	4×10^{-7}	7×10^{-7}	6×10^{-7}	2×10^{-7}	2×10^{-7}	3×10^{-7}	4×10^{-8}	3×10^{-7}	3×10^{-7}	2×10^{-7}	1×10^{-6}
	1×10^{-6}	3×10^{-7}	8×10^{-8}	1×10^{-7}	2×10^{-7}	2×10^{-8}	3×10^{-7}	5×10^{-7}	1×10^{-7}	2×10^{-7}	2×10^{-6}
g	4×10^{-6}	2×10^{-6}	2×10^{-6}	9×10^{-7}	2×10^{-7}	8×10^{-7}	3×10^{-7}	7×10^{-7}	1×10^{-6}	3×10^{-7}	3×10^{-6}
	5×10^{-6}	2×10^{-6}	9×10^{-7}	1×10^{-7}	1×10^{-7}	9×10^{-7}	8×10^{-7}	5×10^{-7}	9×10^{-7}	6×10^{-7}	1×10^{-6}
	4×10^{-6}	2×10^{-6}	1×10^{-6}	8×10^{-7}	6×10^{-7}	1×10^{-6}	5×10^{-7}	1×10^{-6}	2×10^{-6}	4×10^{-7}	4×10^{-6}
θ	2×10^{-6}	2×10^{-6}	2×10^{-6}	1×10^{-6}	3×10^{-7}	7×10^{-7}	1×10^{-6}	1×10^{-6}	5×10^{-8}	1×10^{-6}	4×10^{-6}
	1×10^{-6}	1×10^{-6}	7×10^{-7}	1×10^{-7}	6×10^{-7}	9×10^{-7}	1×10^{-7}	9×10^{-7}	1×10^{-6}	1×10^{-6}	4×10^{-7}
	9×10^{-7}	1×10^{-6}	6×10^{-7}	8×10^{-7}	8×10^{-7}	4×10^{-7}	2×10^{-7}	6×10^{-7}	3×10^{-7}	2×10^{-7}	2×10^{-6}
ϕ	4×10^{-6}	1×10^{-6}	4×10^{-7}	3×10^{-8}	1×10^{-6}	2×10^{-6}	1×10^{-6}	3×10^{-7}	9×10^{-7}	2×10^{-6}	3×10^{-6}
	5×10^{-6}	9×10^{-7}	1×10^{-6}	9×10^{-7}	2×10^{-7}	5×10^{-7}	1×10^{-6}	4×10^{-7}	6×10^{-7}	1×10^{-6}	4×10^{-6}
	5×10^{-6}	4×10^{-8}	2×10^{-6}	1×10^{-6}	2×10^{-7}	9×10^{-7}	1×10^{-6}	4×10^{-7}	4×10^{-7}	7×10^{-7}	1×10^{-6}

model based exponential sheet using the DNN through the radial basis activation function along with the optimization of Bayesian regularization.

The graphs of AE for parameters f, g, θ and ϕ of the fluid dynamics model based exponential sheet are drawn in Table 2 using the DNN through the radial basis activation function along with the optimization of Bayesian regularization. These performances have been plotted between 0 and 1 using 0.1 step size. The best measures of the AE for the classes f, g, θ and ϕ are calculates as 10^{-06} to 10^{-09} of the fluid dynamics model based exponential sheet using the stochastic scheme.

5. Conclusions

The current investigations provide the numerical solutions of fluid dynamics nonlinear system by applying the deep neural network process. The linear and exponential stretching sheets on magneto-rotating Maxwell nanofluid have been presented to the Buongiorno model using the impacts of uneven heat source/sink, varying thermal conductivity and reactive species. The coupled ordinary differential models based on momentum, energy and mass have been obtained through the similarity transformations. The exponential stretching sheet model has been numerically solved by using a novel radial basis activation function together with the Bayesian regularization deep neural network. The deep neural network process is divided into two hidden layers, which has taken thirteen and twenty-five neurons in 1st and 2nd layer. The dataset is proposed using the Runge-Kutta technique of the fluid system. The correctness of the stochastic RB-BRDNN has been obtained using the comparison of proposed and database results. The exact overlapping of the solutions indicates the correctness of the procedure. The negligible values of the absolute error enhance the competence of the stochastic scheme. The competence and reliability of the designed stochastic RB-BRDNN procedure is observed through the error histograms, state transitions, correlation, and regression.

In future, the procedure based on deep neural network along with the radial basis activation function and Bayesian regularization can be implemented to get the performances of various nonlinear models (Baskonus et al., 2019; Yokuş and Gülbahar, 2019; İlhan and Kıymaz, 2020; Brzeziński, 2018; Khalique and Mhlanga, 2018; Khan et al., 2020; Khan et al., 2022; Rehman et al., 2022).

Declaration of Competing Interest

The authors declare that they have no known competing financial interests or personal relationships that could have appeared to influence the work reported in this paper.

Acknowledgement

References

Ahmad, S., Khan, M.N., Nadeem, S., Rehman, A., Ahmad, H., Ali, R., 2021. Impact of Joule heating and multiple slips on a Maxwell nanofluid flow past a slendering surface. Commun. Theor. Phys. 74, (1) 015001.

Ahmad, S., Naveed Khan, M., Nadeem, S., 2022. Unsteady three dimensional bioconvective flow of Maxwell nanofluid over an exponentially stretching sheet with variable thermal conductivity and chemical reaction. Int. J. Ambient Energy 43 (1), 6542–6552.

Ahmed, A., Khan, M., Ahmed, J., 2020. Mixed convective flow of Maxwell nanofluid induced by vertically rotating cylinder. Appl. Nanosci. 10 (12), 5179–5190.

Ali, A., Shehzadi, K., Sulaiman, M., Asghar, S., 2019. Heat and mass transfer analysis of 3D Maxwell nanofluid over an exponentially stretching surface. Phys. Scr. 94, (6) 065206.

Asghar, A., Chandio, A.F., Shah, Z., Vrinceanu, N., Deebani, W., Shutaywi, M., Lund, L.A., 2023. Magnetized mixed convection hybrid nanofluid with effect of heat generation/absorption and velocity slip condition. Heliyon.

Ayub, A., Sabir, Z., Le, D.N., Aly, A.A., 2021. Nanoscale heat and mass transport of magnetized 3-D chemically radiative hybrid nanofluid with orthogonal/inclined magnetic field along rotating sheet. Case Stud. Therm. Eng. 26, 101193.

Ayub, A., Sabir, Z., Altamirano, G.C., Sadat, R., Ali, M.R., 2022. Characteristics of melting heat transport of blood with time-dependent cross-nanofluid model using Keller-Box and BVP4C method. Eng. Comput. 38 (4), 3705–3719.

Baskonus, H.M., Bulut, H., Sulaiman, T.A., 2019. New complex hyperbolic structures to the lonngren-wave equation by using sine-gordon expansion method. Appl. Math. Nonlinear Sci. 4 (1), 129–138.

Brzeziński, D.W., 2018. Review of numerical methods for NumILPT with computational accuracy assessment for fractional calculus. Appl. Math. Nonlinear Sci. 3 (2), 487–502.

Chang, C.L., Lee, Z.Y., 2008. Free convection on a vertical plate with uniform and constant heat flux in a thermally stratified micropolar fluid. Mech. Res. Commun. 35 (6), 421–427.

Daniel, Y.S., Aziz, Z.A., Ismail, Z., Salah, F., 2018. Thermal stratification effects on MHD radiative flow of nanofluid over nonlinear stretching sheet with variable thickness. J. Comput. Des. Eng. 5 (2), 232–242.

De Rochefort, L., Liu, T., Kressler, B., Liu, J., Spincemaille, P., Lebon, V., Wu, J., Wang, Y., 2010. Quantitative susceptibility map reconstruction from MR phase data using bayesian regularization: validation and application to brain imaging. Magn. Reson. Med.: Official J. Int. Soc. Magn. Resonance Med. 63 (1), 194–206.

Farooq, U., Lu, D., Munir, S., Ramzan, M., Suleman, M., Hussain, S., 2019. MHD flow of Maxwell fluid with nanomaterials due to an exponentially stretching surface. Sci. Rep. 9 (1), 1–11.

Hafeez, A., Khan, M., Ahmed, J., 2020. Stagnation point flow of radiative Oldroyd-B nanofluid over a rotating disk. Comput. Methods Programs Biomed. 191, 105342.

Hossain, M.A., Rees, D.A.S., 1999. Combined heat and mass transfer in natural convection flow from a vertical wavy surface. Acta Mech. 136 (3), 133–141.

Ibrahim, W., Makinde, O.D., 2013. The effect of double stratification on boundary-layer flow and heat transfer of nanofluid over a vertical plate. Comput. Fluids 86, 433–441.

Ibrahim, W., Seyoum, J., 2019. Magnetohydrodynamic flow of three-dimensional rotating flow of Sisko fluid past stretching surface with nanoparticles. J. Nanofluids 8 (7), 1412–1422.

İlhan, E., Kıymaz, İ.O., 2020. A generalization of truncated M-fractional derivative and applications to fractional differential equations. Appl. Math. Nonlinear Sci. 5 (1), 171–188.

Kayri, M., 2016. Predictive abilities of bayesian regularization and Levenberg–Marquardt algorithms in artificial neural networks: a comparative empirical study on social data. Math. Comput. Appl. 21 (2), 20.

Khalique, C.M., Mhlanga, I.E., 2018. Travelling waves and conservation laws of a (2 + 1)-dimensional coupling system with Korteweg-de Vries equation. Appl. Math. Nonlinear Sci. 3 (1), 241–254.

Khan, M.N., Ahmad, S., Nadeem, S., Sherif, E.S.M., Ahmad, H., Thounthong, P. and Rehman, A., 2021. Unsteady flow of three-dimensional Maxwell nanofluid with variables properties over a stretching surface. Proceedings of the Institution of Mechanical Engineers, Part E: *Journal of Process Mechanical Engineering*, p.09544089211039055.

Khan, W.A., Irfan, M., Khan, M., 2017. An improved heat conduction and mass diffusion models for rotating flow of an Oldroyd-B fluid. Results Phys. 7, 3583–3589.

Khan, Z.H., Khan, W.A., Tang, J., Sheremet, M.A., 2020. Entropy generation analysis of triple diffusive flow past a horizontal plate in porous medium. Chem. Eng. Sci. 228, 115980.

Khan, Z.H., Khan, W.A., Sheremet, M.A., Hamid, M., Du, M., 2021. Irreversibilities in natural convection inside a right-angled trapezoidal cavity with sinusoidal wall temperature. Phys. Fluids 33, (8) 083612.

Khan, Z.H., Khan, W.A., Qasim, M., Du, M., 2022. Double-diffusive flow in a porous right-angle trapezoidal enclosure with constant heat flux. Math. Methods Appl. Sci. 45 (6), 3305–3317.

Khan, Z.H., Khan, W.A., Qasim, M., Alharbi, S.O., Hamid, M., Du, M., 2022. Hybrid nanofluid flow around a triangular-shaped obstacle inside a split lid-driven trapezoidal cavity. Eur. Phys. J. Spec. Top. 231 (13), 2749–2759.

Khan, M., Malik, M.Y., Salahuddin, T., Khan, F., 2019. Generalized diffusion effects on Maxwell nanofluid stagnation point flow over a stretchable sheet with slip conditions and chemical reaction. J. Braz. Soc. Mech. Sci. Eng. 41 (3), 1–9.

Khan, M.N., Nadeem, S., 2020. Theoretical treatment of bio-convective Maxwell nanofluid over an exponentially stretching sheet. Can. J. Phys. 98 (8), 732–741.

Khan, M.N., Akkurt, N., Ahammad, N.A., Ahmad, S., Amari, A., Eldin, S.M., Pasha, A.A., 2022. Irreversibility analysis of Ellis hybrid nanofluid with surface catalyzed reaction and multiple slip effects on a horizontal porous stretching cylinder. Arabian J. Chem. 15, (12) 104326.

Khan, M.N., Nadeem, S., 2021. A comparative study between linear and exponential stretching sheet with double stratification of a rotating Maxwell nanofluid flow. Surf. Interfaces 22, 100886.

Khan, I., Raja, M.A.Z., Shoaib, M., Kumam, P., Alrabaiah, H., Shah, Z., Islam, S., 2020. Design of neural network with Levenberg-Marquardt and Bayesian regularization backpropagation for solving pantograph delay differential equations. IEEE Access 8, 137918–137933.

Khan, I., Raja, M.A.Z., Khan, M.A.R., Shoaib, M., Islam, S., Shah, Z., 2022. Design of backpropagated intelligent networks for nonlinear second-order Lane-Emden pantograph delay differential systems. Arabian J. Sci. Eng. 47 (2), 1197–1210.

Khan, Z.H., Usman, M., Khan, W.A., Hamid, M., Haq, R.U., 2022. Thermal treatment inside a partially heated triangular cavity filled with casson fluid with an inner cylindrical obstacle via FEM approach. Eur. Phys. J. Spec. Top. 231 (13), 2683–2694.

Khan, N.S., Zuhra, S., Shah, Z., Bonyah, E., Khan, W., Islam, S., Khan, A., 2019. Hall current and thermophoresis effects on magnetohydrodynamic mixed convective heat and mass transfer thin film flow. J. Phys. Commun. 3, (3) 035009.

Kumar, P., Merchant, S.N., Desai, U.B., 2004. Improving performance in pulse radar detection using Bayesian regularization for neural network training. Digital Signal Process 14 (5), 438–448.

Lakshmi, K.S. Sarojamma, G. Makinde, O. D., 2018. Dual stratification on the Darcy-Forchheimer flow of a Maxwell nanofluid over a stretching surface, in: Defect and Diffusion Forum, 387, Trans Tech Publications Ltd, pp. 207–217.

Lin, Y., Lee, D.D., 2006. Bayesian regularization and nonnegative deconvolution for room impulse response estimation. IEEE Trans. Signal Process 54 (3), 839–847.

Maxwell, J.C., 2003. On the dynamical theory of gases. In The kinetic theory of gases: an anthology of classic papers with historical commentary (pp. 197-261).

Mukhopadhyay, S. and Ishak, A., 2012. Mixed convection flow along a stretching cylinder in a thermally stratified medium. J. Appl. Math, 2012.

Nadeem, S., Haq, R.U., Khan, Z.H., 2014. Numerical study of MHD boundary layer flow of a Maxwell fluid past a stretching sheet in the presence of nanoparticles. J. Taiwan Inst. Chem. Eng. 45 (1), 121–126.

Nadeem, S., Ahmad, S., Muhammad, N., Mustafa, M.T., 2017. Chemically reactive species in the flow of a Maxwell fluid. Results Phys. 7, 2607–2613.

Nawaz, M., Rafiq, S., Qureshi, I.H., Saleem, S., 2020. Combined effects of partial slip and variable diffusion coefficient on mass and heat transfer subjected to chemical reaction. Phys. Scr. 95, (3) 035222.

Nazar, R., Amin, N., Pop, I., 2004. Unsteady boundary layer flow due to a stretching surface in a rotating fluid. Mech. Res. Commun. 31 (1), 121–128.

Rakhshkhorshid, M., Teimouri Sendesi, S.A., 2014. Bayesian regularization neural networks for prediction of austenite formation temperatures (Ac1 and Ac3). J. Iron. Steel Res. Int. 21 (2), 246–251.

Rashid, S., Khan, M.I., Hayat, T., Ayub, M., Alsaedi, A., 2020. Numerical treatment for rotating Maxwell nanomaterial flow with Arrhenius energy. Appl. Nanosci. 10 (8), 2665–2672.

Rehman, K.U., Çolak, A.B., Shatanawi, W., 2022. Artificial neural networking (ANN) model for drag coefficient optimization for various obstacles. Mathematics 10 (14), 2450.

Rehman, K.U., Shatanawi, W., Çolak, A.B., 2023. Computational analysis on magnetized and non-magnetized boundary layer flow of casson fluid past a cylindrical surface by using artificial neural networking. Mathematics 11 (2), 326.

Rehman, K.U., Shatanawi, W., Çolak, A.B., 2023. Artificial neural networking estimation of skin friction coefficient at cylindrical surface: a Casson flow field. Eur. Phys. J. Plus 138 (1), 1–15.

Rehman, K.U., Shatanawi, W., Çolak, A.B., 2023. Artificial neural networking magnification for heat transfer coefficient in convective non-newtonian fluid with thermal radiations and heat generation effects. Mathematics 11 (2), 342.

Sabir, Z., 2022. Neuron analysis through the swarming procedures for the singular two-point boundary value problems arising in the theory of thermal explosion. Eur. Phys. J. Plus 137 (5), 638.

Sabir, Z., 2022. Stochastic numerical investigations for nonlinear three-species food chain system. Int. J. Biomath. 15 (04), 2250005.

Sabir, Z., Umar, M., Raja, M.A.Z., Baskonus, H.M. and Gao, W., 2021. Designing of Morlet wavelet as a neural network for a novel prevention category in the HIV system. Int. J. Biomath, p.2250012

Sabir, Z., Wahab, H.A., Javeed, S., Baskonus, H.M., 2021. An efficient stochastic numerical computing framework for the nonlinear higher order singular models. Fractal Frac. 5 (4), 176.

Sajid, T., Tanveer, S., Sabir, Z. and Guirao, J.L.G., 2020. Impact of activation energy and temperature-dependent heat source/sink on maxwell–sutterby fluid. Math. Probl. Eng, 2020

Saleem, S., Qasim, M., Alderremy, A., Noreen, S., 2020. Heat transfer enhancement using different shapes of Cu nanoparticles in the flow of water based nanofluid. Phys. Scr. 95, (5) 055209.

Sandeep, N., Gnaneswara Reddy, M., 2017. MHD Oldroyd-B fluid flow across a melting surface with cross diffusion and double stratification. Eur. Phys. J. Plus 132 (3), 1–18.

Shafique, Z., Mustafa, M., Mushtaq, A., 2016. Boundary layer flow of Maxwell fluid in rotating frame with binary chemical reaction and activation energy. Results Phys. 6, 627–633.

Shah, Z., Ullah, A., 2023. Ferrofluid treatment with insertion of electric field inside a porous cavity considering forced convection. Waves Random Complex Medium, 1–19.

Shah, Z., Rooman, M., Shutaywi, M., 2023. Computational analysis of radiative engine oil-based Prandtl-Eyring hybrid nanofluid flow with variable heat transfer using the Cattaneo-Christov heat flux model. RSC Adv. 13 (6), 3552–3560.

Shateyi, S., 2013. A new numerical approach to MHD flow of a Maxwell fluid past a vertical stretching sheet in the presence of thermophoresis and chemical reaction. Boundary Value Probl. 2013 (1), 1–14.

Singh, V., Agarwal, S., 2014. MHD flow and heat transfer for Maxwell fluid over an exponentially stretching sheet with

variable thermal conductivity in porous medium. Therm. Sci. 18 (suppl. 2), 599–615.

Sulochana, C., Ashwinkumar, G.P. and Sandeep, N., 2017. Effect of thermophoresis and Brownian moment on 2D MHD nanofluid flow over an elongated sheet. In Defect and Diffusion Forum (Vol. 377, pp. 111-126). *Trans Tech Publications Ltd.*

Tang, T.Q., Rooman, M., Shah, Z., Jan, M.A., Vrinceanu, N., Racheriu, M., 2023. Computational study and characteristics of magnetized gold-blood Oldroyd-B nanofluid flow and heat transfer in stenosis narrow arteries. J. Magn. Magn. Mater. 170448

Tlili, I., Naseer, S., Ramzan, M., Kadry, S., Nam, Y., 2020. Effects of chemical species and nonlinear thermal radiation with 3D Maxwell nanofluid flow with double stratification—an analytical solution. Entropy 22 (4), 453.

Umar, M., Sabir, Z., Raja, M.A.Z., Sánchez, Y.G., 2020. A stochastic numerical computing heuristic of SIR nonlinear model based on dengue fever. Results Phys. 19, 103585.

Wang, C.Y., 1988. Stretching a surface in a rotating fluid. Zeitschrift Angew. Math. Phys. ZAMP 39 (2), 177–185.

Wang, F., Ahmad, S., Al Mdallal, Q., Alammari, M., Khan, M.N., Rehman, A., 2022. Natural bio-convective flow of Maxwell nanofluid over an exponentially stretching surface with slip effect and convective boundary condition. Sci. Rep. 12 (1), 2220.

Yokuş, A., Gülbahar, S., 2019. Numerical solutions with linearization techniques of the fractional Harry Dym equation. Appl. Math. Nonlinear Sci. 4 (1), 35–42.